Compression field modeling of confined concrete

E. Montoya†, F.J. Vecchio‡ and S.A. Sheikh‡

Department of Civil Engineering, University of Toronto, Toronto, Canada

Abstract. The three-dimensional behavior of confined concrete was investigated, including strength enhancement due to triaxial compressive stresses, lateral expansion, compression softening, cover spalling and post-peak ductility. A finite element program based on a nonlinear elasticity methodology was employed to evaluate the ability to model triaxial behavior of reinforced concrete (RC) by combining constitutive models proposed by several researchers. The capability of compression field based models to reproduce the softening behavior of lightly cracked confined concrete was also investigated. Data from tested specimens were used to evaluate the validity of the formulations. Good agreement with the experimental results was obtained.

Key words: nonlinear; finite element; analysis; reinforced concrete; confinement; lateral expansion; columns.

1. Introduction

A wide variety of constitutive material models that take into account the influence of triaxial states of strain and stress have been developed for RC. Modeling of RC columns ranges from empirical models based on experimental results to nonlinear finite element analysis (NLFEA) based on fracture mechanics or plasticity (Chen 1982).

Stress-strain formulations for confined concrete have been derived from axially loaded columns tested under different load rates. Some of the parameters that have been studied are: unconfined concrete strength; volumetric ratio of lateral steel; longitudinal reinforcement arrangements; tie setup; lateral steel spacing; and cover dimensions (Sheikh and Uzumeri 1980, Scott *et al.* 1982, Mander *et al.* 1988, Cusson and Paultre 1995, Rasvi and Saatcioglu 1999). The analytical stress-strain curves typically fit with great accuracy the sets of columns tested by their own authors, but sometimes they lack general applicability. These models are largely empirical in nature and their formulation includes parameters not convenient for finite element analysis.

Using an entirely different approach, several researchers have studied triaxial behavior of concrete using formulations based on fracture mechanics or plasticity. For example, University of Alberta researchers (Xie *et al.* 1996) implemented the model of Pramono and Willam (1989) in a finite element code to reproduce the results of four columns tested. Parameters were adjusted for high strength concrete (HSC), and a new definition for "crack spacing" as a function of principal stress accounted for less stiffened HSC Columns with moderate confinement. Although good agreement was reached, some difficulties arose from the lack of automation in load increments within the

† Ph.D. Candidate
‡ Professor

program.

Karibanis and Kiousis (1994) used a Drucker-Prager model to analyze the behavior of columns confined with either ties or spirals. The model included a nonassociative flow rule, strain hardening, and a limited tensile strength for the concrete. Elastoplastic stress increments were computed using a rather complicated constitutive matrix that was evaluated numerically. In this model, different confining zones between ties or spirals were defined. The applicability of the model included only circular columns.

Models derived from fracture mechanics and plasticity generally show good agreement with experimental results, but difficulties often arise in their numerical implementation. As well, they do not always capture a wide spectrum of possible three-dimensional behavior of RC. On the other hand, description of empirical models are based on physical variables often used for practical design of RC elements, but their formulation is not always suitable for NLFEA.

The analytical methodology presented in this study for the modeling of confined concrete follows a nonlinear-elastic based approach, which bridges the practicability of empirical material relationships with theoretically-oriented mechanics-based formulations combining good points of each.

An initial attempt in this direction to model confined concrete was made by Selby (1990) and Selby and Vecchio (1993). The plasticity model by Hsieh *et al.* (see Chen 1982) along with empirical stress-strain curves for concrete were implemented in a nonlinear elastic-based finite element program. Cracked concrete was modeled as an orthotropic material with rotating smeared cracks. The nonlinear elastic analyses were carried out updating the secant stiffness material matrices for both concrete and steel. Six of the columns tested by Sheikh and Uzumeri (1980) were modeled with an enhanced version of the program, but difficulties arose when modeling the post-peak behavior of well-confined columns due to the lack of smooth transitions between triaxial compressive states and triaxial tensile states, and the aspect ratio of the meshes. Modeling of cover spalling was not possible.

In this study, the Modified Compression Field Theory (Vecchio and Collins 1986) was employed to model columns subjected to concentric monotonic axial load. Initially used for modeling of cracked concrete (panels, beams), the capability of the MCFT to represent the behavior of confined concrete subjected to triaxial states of stress was explored.

Concrete can be considered confined when subjected to triaxial compression; the triaxial compression increases the concrete's capacity to sustain larger compressive strengths and deformations. When an element of concrete is laterally reinforced (e.g., by ties, hoops or spirals) and subjected to concentric axial compression, lateral expansion of the element in the plane perpendicular to the load activates the lateral steel, which confines the element by exerting lateral pressure. Confined concrete generally fails in a ductile manner, whereas unconfined concrete fails in a brittle manner. As tensile strains develop in unconfined concrete subjected to compression, concrete softens and strength decreases. It is also known that Poisson's ratio does not remain constant but progressively increases as load increases. This phenomenon is beneficial in activating the lateral reinforcement.

Program VecTor3 was used to carry out the analyses. It is a nonlinear elastic finite element program being developed at the University of Toronto based on that of Selby and Vecchio (1993, 1997) for the analysis of reinforced concrete solids. It will be shown that the analytical models implemented reproduce pre- and post-peak behaviors of RC columns subjected to axial compression with reasonable accuracy. Activation of lateral steel, lateral expansion of the concrete core, cracking

and spalling of the concrete cover, yielding of the longitudinal steel, strength enhancement due to confinement, and load resistance at large deformations are captured well. The capabilities of the analytical models are also examined by reproducing the shear stress-lateral displacement behavior of a wall tested under concentric compression and lateral imposed displacements.

2. Material models

The material models used in this study are described below. Stress-strain curves for concrete and steel, and criteria for confinement, cracking, softening, and variable Poisson's ratio of concrete implemented in VecTor3 are presented.

2.1 Stress-strain relationships for concrete in compression

Two base curves were used. The Hognestad parabola (Collins and Mitchell 1997):

$$f_{ci}=f_p\left(2\frac{\varepsilon_{ci}}{\varepsilon_p}-\left(\frac{\varepsilon_{ci}}{\varepsilon_p}\right)^2\right) \tag{1}$$

was implemented for the pre-peak regime (i.e., ascending branch) until the peak stress f_p and peak strain ε_p are reached. In Eq. (1) f_{ci} and ε_{ci} are the compressive stress and strain in the principal i-direction respectively. For the post-peak regime (i.e., descending branch) the Popovics' curve (1973) was used, as follows:

$$f_{ci}=f_p\frac{\left(\frac{\varepsilon_{ci}}{\varepsilon_p}\right)n}{n-1+\left(\frac{\varepsilon_{ci}}{\varepsilon_p}\right)^n} \tag{2}$$

Where n is defined as:

$$n=\frac{E_c}{E_c-E_{\text{sec}}} \tag{3}$$

$$E_{\text{sec}}=\frac{f_p}{\varepsilon_p} \tag{4}$$

E_{sec} is the secant stiffness at peak stress, and the initial tangent stiffness is (in MPa):

$$E_c=5000\sqrt{f_c'} \tag{5}$$

Both relationships are schematically presented in Fig. 1.

2.2 Stress-strain relationship for concrete in tension

Concrete is assumed to follow a linear ascending branch up to the tensile strength f_t'. The strain ε_{cr} at cracking stress is given as:

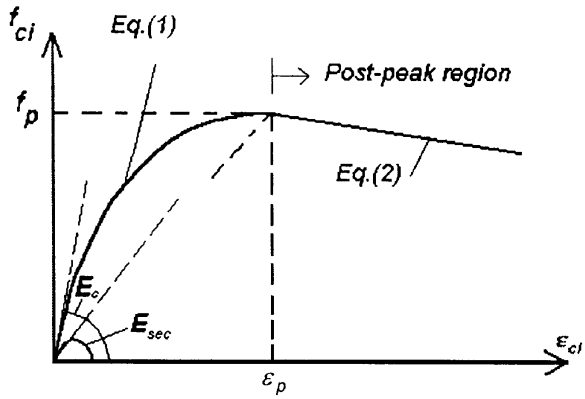

Fig. 1 Stress-strain relationships for concrete in compression

$$\varepsilon_{cr}=\frac{f_t'}{E_c} \tag{6}$$

Cracks are considered smeared within the reinforced concrete, average tensile stresses after reaching f_t' can be calculated due to tension stiffening. The tension stiffening model proposed by Collins and Mitchell (1997) was used:

$$f_{ci}=\frac{f_t'}{1+\sqrt{500\varepsilon_{ci}}} \tag{7}$$

Where ε_{ci} must be a principal tensile strain in the direction under consideration. It is to be noted that the tension-stiffening model is limited by yielding of reinforcement at crack locations.

2.3 Strength enhancement

Once the base stress-strain curves for concrete in compression have been defined, the confined stress, f_p (i.e., peak stress) and its corresponding strain, ε_p, are computed using the following criterion proposed by Vecchio (1992).

A *stress enhancement factor* K_c is defined as:

$$K_c=\left[1.0+0.92\frac{f_{cn}}{f_c'}-0.76\left(\frac{f_{cn}}{f_c'}\right)^2\right]+4.0\frac{(-f_{c1})}{f_c'} \tag{8}$$

where

$$f_{cn}=-(f_{c2}-f_{c1}) \tag{9}$$

Eqs. (8) and (9) are valid If $\mathbf{0} > f_{c1} > f_{c2} > f_{c3}$, where f_{c1},f_{c2} and f_{c3} are principal stresses.

2.4 Cracking criterion

The Mohr-Coulomb criterion was used to account for the cracking stress f_{cr} under triaxial conditions. Its formulation is given below:

$$0.25f_t' \le f_{cr} = f_{crf}\left[1+\frac{f_{c3}}{f_c'}\right] \le f_t' \tag{10}$$

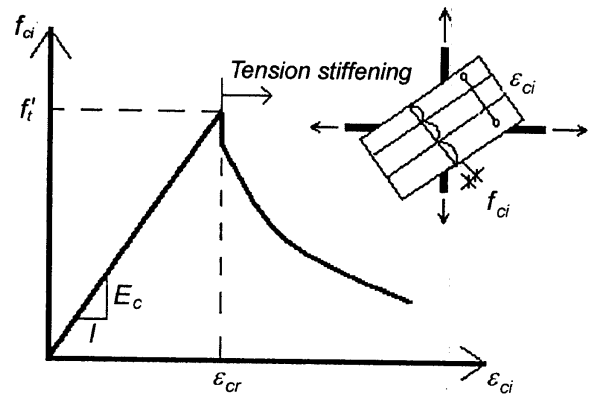

Fig. 2 Stress-strain relationship for concrete in tension

$$f_{crf} = \frac{2c\cos\phi}{1+\sin\phi} \tag{11}$$

Where ϕ is the internal friction angle of concrete (taken as 37°); c is the cohesion, computed as:

$$c = f_c' \frac{1-\sin\phi}{2\cos\phi} \tag{12}$$

and f_c' is the standard cylinder strength of concrete.

2.5 Compression softening of concrete

The MCFT recognized the effects of tensile strains in cracked concrete. As concrete cracks, tensile stresses develop in the concrete between cracks; from zero stress at a crack location to a maximum half way (see Fig. 2). The effect of tensile strains is to reduce the compressive strength in the direction parallel to the cracks.

The tentative model proposed by Vecchio (1992) was used in this study, where the *compression softening factor* K_d is computed as:

$$K_d = \frac{1}{1.0-0.35\left[\frac{\varepsilon_{c1}}{\varepsilon_{ci}} - 0.28\right]^{0.8}} \leq 1.0 \tag{13}$$

Where ε_{c1} is the tensile strain in the direction normal to the compressive strain ε_{ci}. It is assumed in the MCFT that corresponding principal strains and stresses have the same direction.

The peak compressive stress and the strain at peak stress are calculated as:

$$f_p = K_c K_d f_c' \tag{14}$$

$$\varepsilon_p = K_c K_d \varepsilon_o \tag{15}$$

Where f_c' is the standard cylinder strength of concrete, and ε_o is the peak strain at f_c', and K_c is the *stress enhancement factor* defined above.

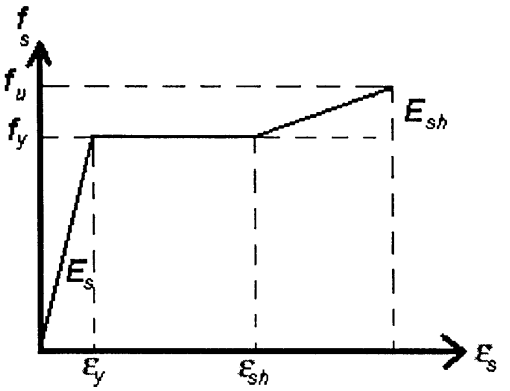

Fig. 3 Stress-strain relationship for steel

2.6 Variable Poisson's ratio

It has been shown (Montoya 2000) that the Poisson's ratio v varies with increments in the axial strain for the case of columns subjected to concentric axial compression. The tentative expression used in the finite element modeling is:

$$v_{ji}=v_o\left[1.0+1.5\left(2.0\frac{\varepsilon_{ci}}{\varepsilon_o}-1.0\right)^2\right]\leq 0.5 \tag{16}$$

where v_{ji} is the Poisson's ratio in the j-direction due to stress in the i-direction, v_o is the initial Poisson's ratio. This equation was a slightly modified version of that proposed by Vecchio (1992).

2.7 Stress-strain curve for steel

The monotonic response of steel was modeled with a simple elasto-plastic model with strain hardening, as shown in Fig. 3. Where ε_y is the yielding strain, ε_{sh} is the strain at hardening, E_s is the initial stiffness, E_{sh} is the strain hardening modulus, f_y is the yielding stress and f_u is the rupture stress. The model was considered valid for either compressive or tensile stresses.

3. Finite element models

3.1 Program VecTor3

Program VecTor3 is a nonlinear finite element program that has been developed at the University of Toronto for the analysis of reinforced concrete solids.

The 3D stress state is related to the 3D strain state through a constitutive material matrix, as shown below:

$$\{\sigma\}=[D]\{\varepsilon\}-\{\sigma_o\} \tag{17}$$

where $\{\sigma\}$ is the stress vector, $[D]$ is the material stiffness matrix, and $\{\varepsilon\}$ is the strain vector, and $\{\sigma_o\}$ is used to model elastic offsets;

$$\{\sigma_o\}=[D_c]\{\varepsilon_c^o\} \tag{18}$$

where $[\boldsymbol{D_c}]$ is the material stiffness matrix for concrete, and $\{\boldsymbol{\varepsilon_c}^o\}$ is the strain vector to represent Poisson's strains or expansions. An expression to represent elastic offsets in steel will be similar to that of Eq. (18).

The material matrix $[\boldsymbol{D}]$ is given in terms of the secant stiffness moduli, Poisson's ratio $\boldsymbol{\nu}$, and shear moduli $\boldsymbol{G}$ in three directions (i.e., local, global or principal directions). Secant moduli vary at each load state as a function of the stress state.

It is assumed in VecTor3 that concrete behaves isotropically before cracking, and orthotropically afterwards. Cracks are assumed to be smeared within concrete, thus allowing the user to maintain the same finite element mesh during the analysis process, and not having to change it due to localized cracks. Although cracks are assumed smeared, stress checks at crack surfaces are performed to satisfy compatibility and equilibrium.

Steel can be modeled as smeared within the concrete elements, or represented as truss bars attached to solid elements. In any case, perfect bond is assumed between the two materials. Buckling is not taken into account when a truss bar is subjected to compression. Bending is also ignored in its stiffness matrix.

In the material matrix of Eq. (17); $[\boldsymbol{D}]$, comprises the material matrices for concrete and smeared steel, $[\boldsymbol{D_c}]$ and $[\boldsymbol{D_s}]$, respectively (in global coordinates). $[\boldsymbol{D_s}]$ is the sum of the steel material matrices, calculated as:

$$[D_s]=\sum_{i=1}^{n}[D_s]_i \tag{19}$$

where $\boldsymbol{n}$ is the number of steel components. Thus, the total material matrix can be written as:

$$[D]=[D_c]+\sum_{i=1}^{n}[D_s]_i \tag{20}$$

The orthotropic material stiffness matrix used for concrete (Selby and Vecchio 1993) in principal directions is:

$$[D_c']=\begin{bmatrix} E_{c1} & 0 & 0 & 0 & 0 & 0 \\ 0 & E_{c1} & 0 & 0 & 0 & 0 \\ 0 & 0 & E_{c1} & 0 & 0 & 0 \\ 0 & 0 & 0 & G_{c12} & 0 & 0 \\ 0 & 0 & 0 & 0 & G_{c23} & 0 \\ 0 & 0 & 0 & 0 & 0 & G_{c13} \end{bmatrix} \tag{21}$$

where $\boldsymbol{E_{ci}}$ is the secant modulus in the principal direction $\boldsymbol{i}$=1, 2, 3; and $\boldsymbol{G_{ij}}$ is the shear modulus given by

$$G_{cij}=\frac{E_{ci}E_{cj}}{E_{ci}+E_{cj}} \tag{22}$$

The smeared steel material matrix in $\boldsymbol{i}$-direction is given by:

$$[D_s]_i=\begin{bmatrix} \rho_{si}\cdot\frac{f_{si}}{\varepsilon_{si}} & 0 & 0 & 0 & 0 & 0 \\ 0 & 0 & 0 & 0 & 0 & 0 \\ 0 & 0 & 0 & 0 & 0 & 0 \\ 0 & 0 & 0 & 0 & 0 & 0 \\ 0 & 0 & 0 & 0 & 0 & 0 \\ 0 & 0 & 0 & 0 & 0 & 0 \end{bmatrix} \tag{23}$$

where f_{si} and ε_{si} are the stress and strain in the i-direction, respectively, and ρ_{si} is the reinforcement ratio in that direction. It is noted that the secant modulus for steel is determined as:

$$E_{si}=\frac{f_{si}}{\varepsilon_{si}} \tag{24}$$

At any load stage the secant moduli depends on the stress-strain condition in the direction being analyzed. In the case of concrete (see Fig. 4):

$$E_{ci}=\frac{f_{ci}}{\varepsilon_{ci}} \tag{25}$$

where ε_{ci} is the stress-related strain in that direction. Other strains due to prestress, thermal loading or lateral expansion (i.e., Poisson's effect) are introduced as "*prestrains*" (Vecchio 1992) and converted into *equivalent forces*. As lateral expansion changes at each load stage according to the strain state, its related *prestrains* are updated at every iteration.

VecTor3 solves for displacements as in a linear elastic program. The global stiffness matrix is the assembly of element stiffness matrices computed with Eq. (19), and is updated and used to solve for new displacements as load or imposed nodal displacements are incremented.

3.2 Description of the structural elements analyzed with VecTor3

This section shows the geometry and finite element meshes of seven structural elements modeled with the program. Four square columns tested by Sheikh and Uzumeri (1980), a rectangular wall tested by Mander *et al.* (1988), a circular column tested by Liu *et al.* (1998), and a shear wall tested

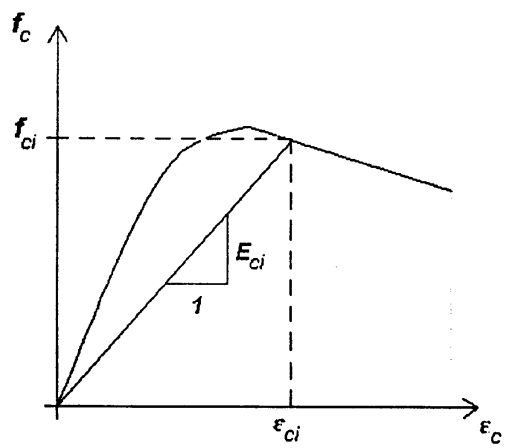

Fig. 4 Secant stiffness

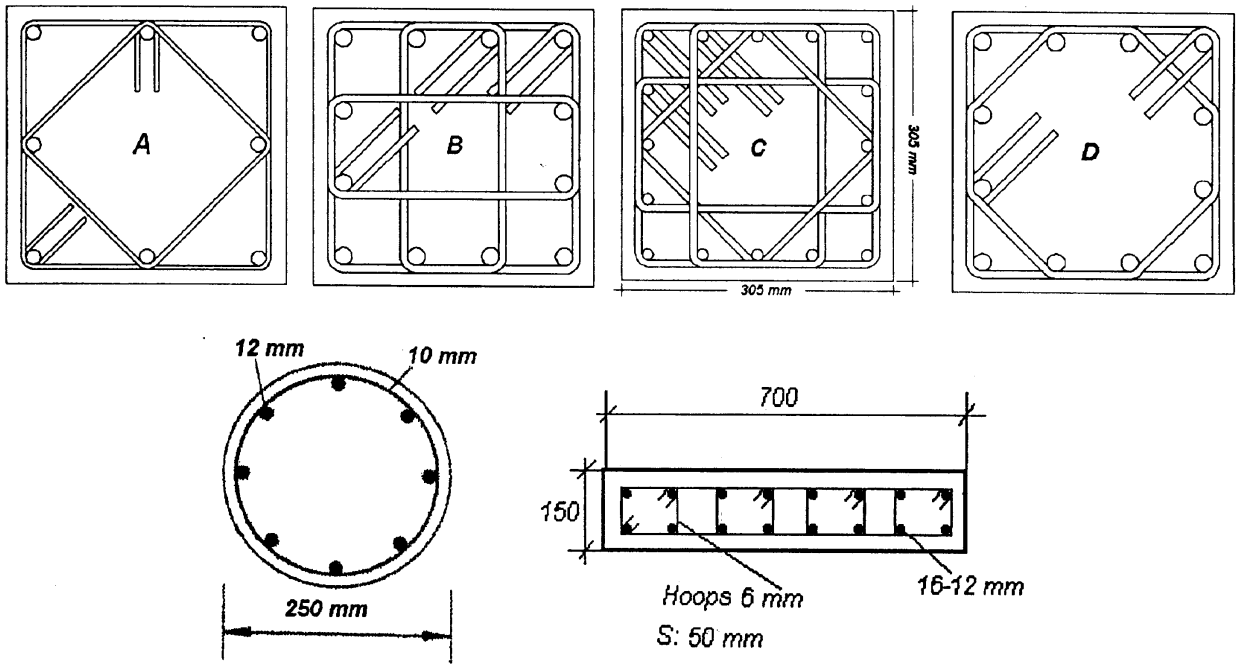

Fig. 5 Cross sections of columns

by Lefas *et al.* (see Vecchio 1992) were considered. All of the structural elements were subjected to axial concentric compression with the exception of the shear wall, which was also subjected to horizontal monotonic load. This selection represented a broad spectrum of cross section shapes, concrete strengths, and lateral steel arrangements.

The column sections are plotted in Fig. 5, and the finite element meshes in Fig. 6. Only one-

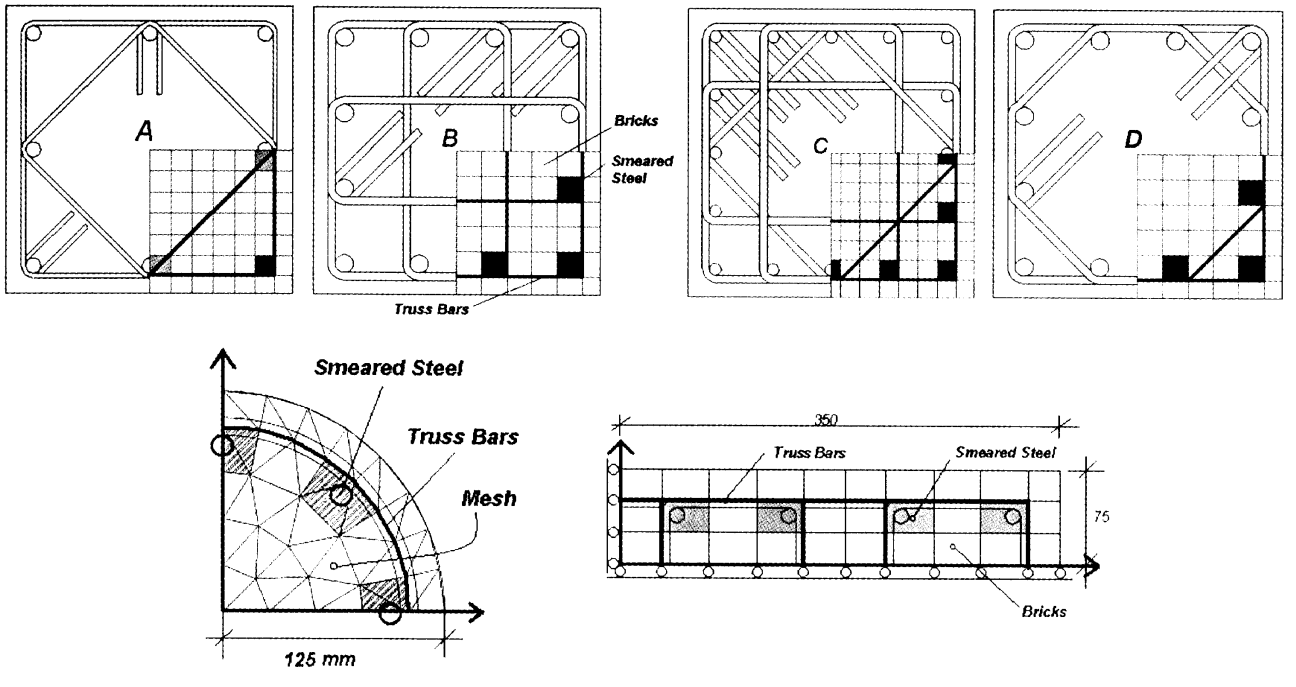

Fig. 6 Plan view of finite element meshes

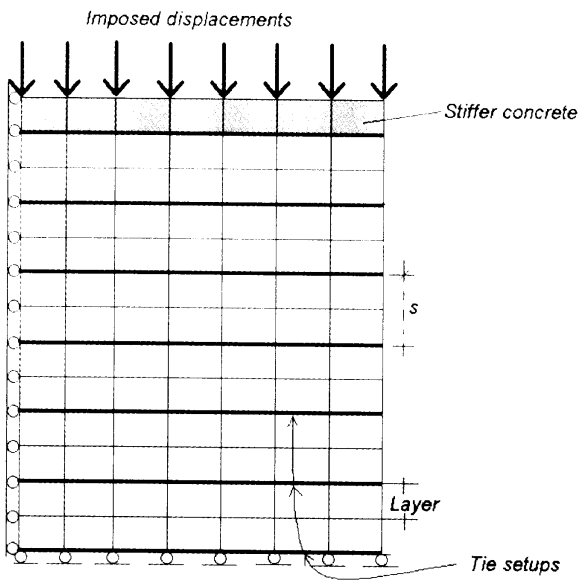

Fig. 7 Vertical view of three-dimensional finite element meshes

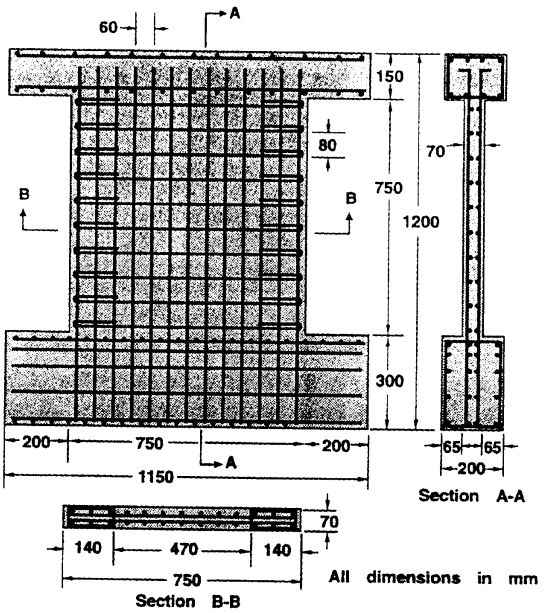

Fig. 8 Wall SW16

quarter of the column's cross sections were modeled due to symmetry. A vertical profile of the three-dimensional mesh is shown in Fig. 7. Eight-noded bricks were used to model the concrete elements of the square and rectangular columns, and six-noded wedges were used to model the circular section. In all the models, truss bars were used to model the ties and hoops, and the longitudinal reinforcement was smeared within the concrete bricks located at the position of each bar. In the case of the Lefas *et al.* wall (SW16), all the reinforcement was embedded within the concrete bricks. The whole wall was modeled due to the asymmetry of the applied load; a plot of the wall and its model is shown in Figs. 8 and 9.

The material properties of the elements are given in Tables 1 to 4, where d_b is the longitudinal bar

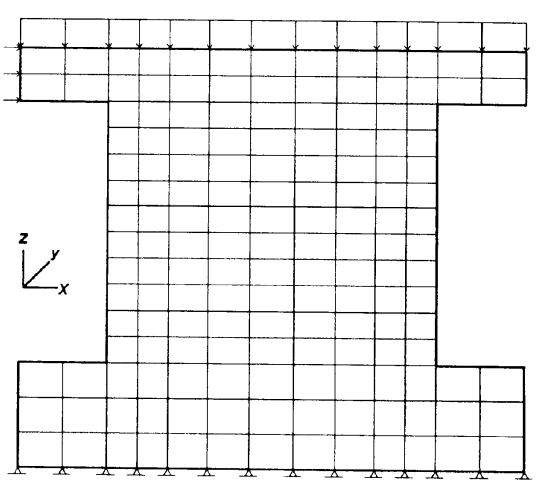

Fig. 9 Finite element mesh for SW16

Table 1 Sheikh and Uzumeri column properties

Specimen		Longitudinal Steel						
Column[a]	Conf. type	d_b [mm]	A_s [mm^2]	ρ_s [%]	f_y [MPa]	E_s [MPa]	E_{sh} [MPa]	ε_{sh} [mm/m]
2A1-1	A	15.875	1600	1.72	367	200000	9220	7.70
4B3-19	B	19.050	3406	3.67	392	196400	6200	7.80
2C5-17	C	12.700	2065	2.22	407	196400	8960	9.10
4D6-24	D	19.050	3406	3.67	392	196400	6200	7.80

Specimen	Tie Steel						Concrete	
Column	d_h [mm]	A_h [mm^2]	ρ_v [%]	f_{yh} [MPa]	E_s [MPa]	s [mm]	f'_c [MPa]	ε_o [mm/m]
2A1-1	4.76	17.8	0.80	540	200000	57.1	37.5	2.2
4B3-19	7.94	49.5	1.80	480	199500	101.6	33.4	2.2
2C5-17	7.94	49.5	2.37	480	200000	101.6	32.9	2.2
4D6-24	6.35	31.7	2.30	480	199500	38.1	35.9	2.2

[a]Column dimensions: 305 × 305 mm

Table 2 Liu *et al.* column properties

Specimen[a]	Tie Steel							Concrete	
2C80-10S50-15	type	d_h [mm]	A_h[b] [mm^2]	ρ_v [%]	f_{yh} [MPa]	E_s [MPa]	s [mm]	f'_c [MPa]	E_c [MPa]
	spiral	10.3	83.3	6.4	660	217000	50	82	46300
Longitudinal Bars		d_b	A_s	ρ_s	f_y	E_s			
		12.1	920	1.8	430	198000			

[a]Column diameter 250 mm
[b]Calculated by the writers

Table 3 Mander *et al.* wall 11 properties

Label	Tie Steel							
Wall 11[a]	type	d_h [mm]	A_h [mm^2]	ρ_v [%]	f_{yh} [MPa]	E_s [MPa]	E_{sh} [MPa]	ε_{sh} [mm/m]	s [mm]
	hoops	6.0	28.3	2.33	310	198000	3200	22.00	50

Longitudinal Steel							Concrete	
d_b [mm]	A_s[b] [mm^2]	ρ_s [%]	f_y [MPa]	E_s [MPa]	E_{sh} [MPa]	ε_{sh} [mm/m]	f'_c [MPa]	E_c [MPa]
16.0	3217	3.06	290	191000	3900	24.00	41	31000
20.0	3770	1.86	434	200000[b]	5000[b]	8.00[b]	24.8	24900[b]

[a]Wall dimension: 700 mm × 150
[b]Calculated or assumed by the writers

Table 4 Material properties of wall SW16

Steel	d_b [mm]	A_s[a] [mm^2]	f_y [MPa]
(1)	(2)	(3)	(4)
Vertical	8.00	50.3	470
Horizontal	6.25	30.7	520
Stirrups	4.00	12.6	420
E_s[b]	210000 [MPa]		
ε_{sh}[b]	2.5 [mm/m]		
f'_c	4.0 [MPa]		

[a] Calculated by the writers
[b] Assumed

diameter, A_s is the total longitudinal bar cross sectional area in the column, ρ_s is the longitudinal steel ratio with respect to the gross section, f_y is the longitudinal steel yielding stress, E_s is the initial steel stiffness, E_{sh} and ε_{sh} are the stiffness modulus and strain at hardening, respectively. Also, d_h and A_h are the tie diameter and area, ρ_v is the volumetric ratio, f_{yh} is the tie yielding stress, s is the spacing between sets of ties. It is to be noted that the plain concrete strength of all the specimens described was taken as $0.85f_c'$, where f_c' is the standard cylinder strength of concrete.

4. Corroboration

The finite element analyses were made using two options: considering or not the effect of compression softening of concrete due to tensile strains in the direction perpendicular to the applied load. It was found that compression softening had little effect on well-confined columns (i.e., with high volumetric ratios and small tie spacings), whereas it did influence the response of poorly-confined elements. It was apparent that these analyses served as upper and lower bounds to the actual observed behavior. The maximum loads obtained from the tests are compared to the

Table 5 Maximum analytical to experimental load ratio

Researcher	Column	P_{max} (test) [kN]	$P_{anal.}$ (VecTor3) (w./soft) [kN]	$P_{anal.}$ (VecTor3) (wo./soft) [kN]	P (VecTor3) / P_{test}	
Sheikh and Uzumeri	2A1-1	3418	3370	3660	0.99	1.07
	2C5-17	3524	3622	4355	1.03	1.24
	4B3-19	4094	4137	4277	1.01	1.04
	4D6-24	4725	4650	4858	0.98	1.03
Liu *et al.*	2C80-10S50-15	3880	3324	3850	0.86	0.99
Mander *et al.*	Wall 11	5000	4260	4857	0.85	0.97
Mean					***0.95***	***1.06***
Std. Dev.					***0.08***	***0.09***

Table 6 Sequence of events in the loading process

Researcher	Column	axial strain[a] @ spalling		tie strain[b] @ P_{max}		axial strain @ P_{max}	
		Exp. [10^{-3}]	Anal. [10^{-3}]	Exp. [10^{-3}]	Anal. [10^{-3}]	Exp. [10^{-3}]	Anal. [10^{-3}]
Sheikh and Uzumeri	2A1-1	1.50 to 2.00	1.52	1.90	1.40	3.60	2.98
	2C5-17	1.50 to 2.00	3.29	1.80	2.40	15.70	8.37
	4B3-19	1.50 to 2.00	1.20 to 1.80	2.30	2.50	6.10	5.50
	4D6-24	1.50 to 2.00	1.60	4.50	5.20	17.70	11.73
Liu *et al.*	2C80-10S50-15	2.80	2.00 to 2.40	0.32 2.50	1.40 (1st peak)[c] 3.20 (2nd peak)	2.90 10.00	3.24 (1st peak)[c] 9.50 (2nd peak)
Mander *et al.*	Wall 11	2.00	1.80	1.57	1.00	3.00[d]	3.60

[a]axial strain compressive
[b]tie strain tensile
[c]average
[d]strain at P_{max}, not ε_{cc} at f_{cc}

analytical peak loads in Table 5; and the sequence of events, such as: axial strain at cracking, tie strain at maximum load, and peak axial strains are compared with the experimental results in Table 6. The analytical loads were found to be between 95% to 106% of the experimental values, with a standard deviation between 8 and 9%.

A graphical representation of Table 5 is shown in Fig. 10. There was no significant difference in the computed values with respect to the experimental ones. Thus, it is apparent that the tentative model for strength enhancement proposed by Vecchio (1992) can be used in the analysis of

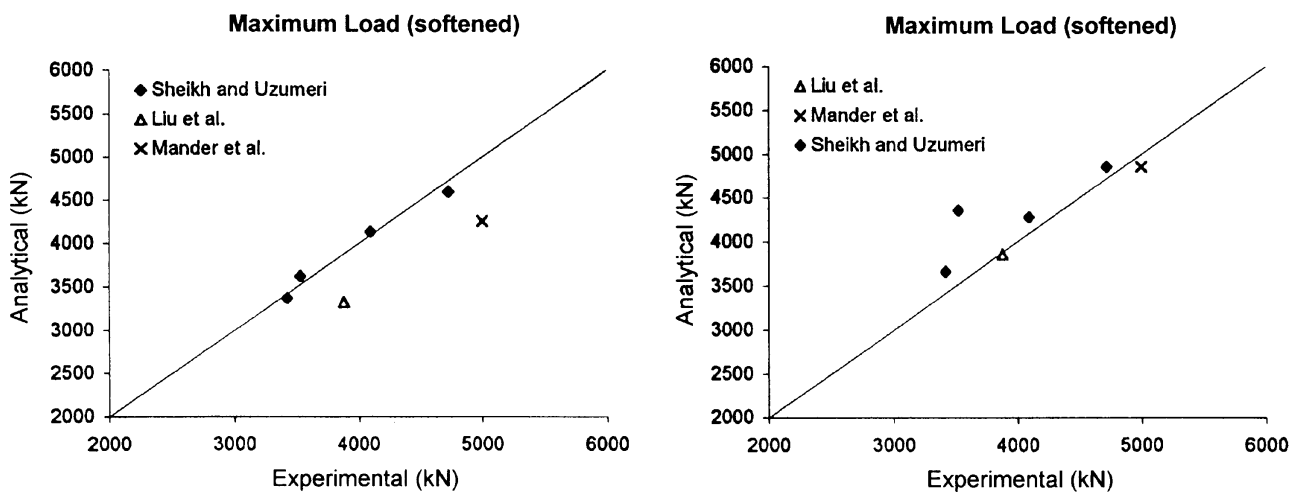

Fig. 10 Maximum analytical to experimental load ratios

confined concrete regardless of the element shape (e.g., circular, rectangular, and square columns), and concrete type (e.g., normal or high strength concrete).

It should also be mentioned that the strength enhancement model represented well the behavior of both core and cover concrete; the tentative lateral pressure formulation (see Eq. 9) clearly identified the difference in stress-strain paths followed by the cover and the core. Whereas three-dimensional compressive stresses were observed in the core concrete in the analytical models in the vicinity of the tie arrangements; lateral tensile stresses produced cracking of concrete covers, and compression softening in the axial direction of the columns. As a result, cover spalling was modeled well in all the columns.

Figs. 11 to 13 show the axial load-axial strain curves for all the columns. As can be seen, the analytical responses traced with reasonable accuracy of the actual behavior of the specimens.

The experimental and analytical shear-lateral displacement curves for the shear wall SW16 are shown in Fig. 14, and a plot of the deformed wall near failure is shown in Fig. 15 (horizontal load applied from left to right). The analytical response was stiffer than the experimental, but the analytical shear strength was 351 kN, which was only 1% smaller than the actual (the wall shear

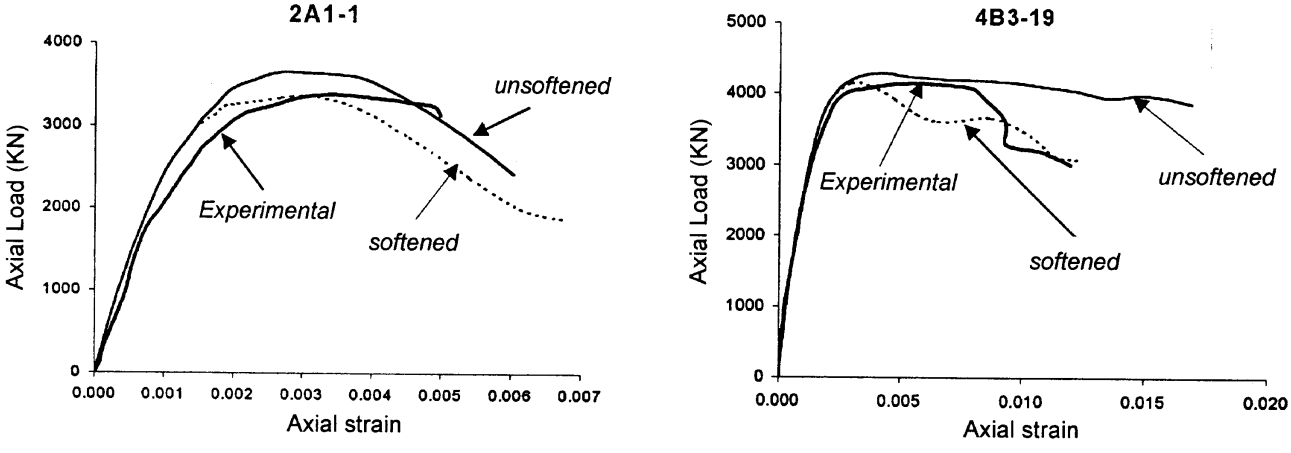

Fig. 11 Axial load-axial strain curves for 2A1-1 and 4B3-19 columns

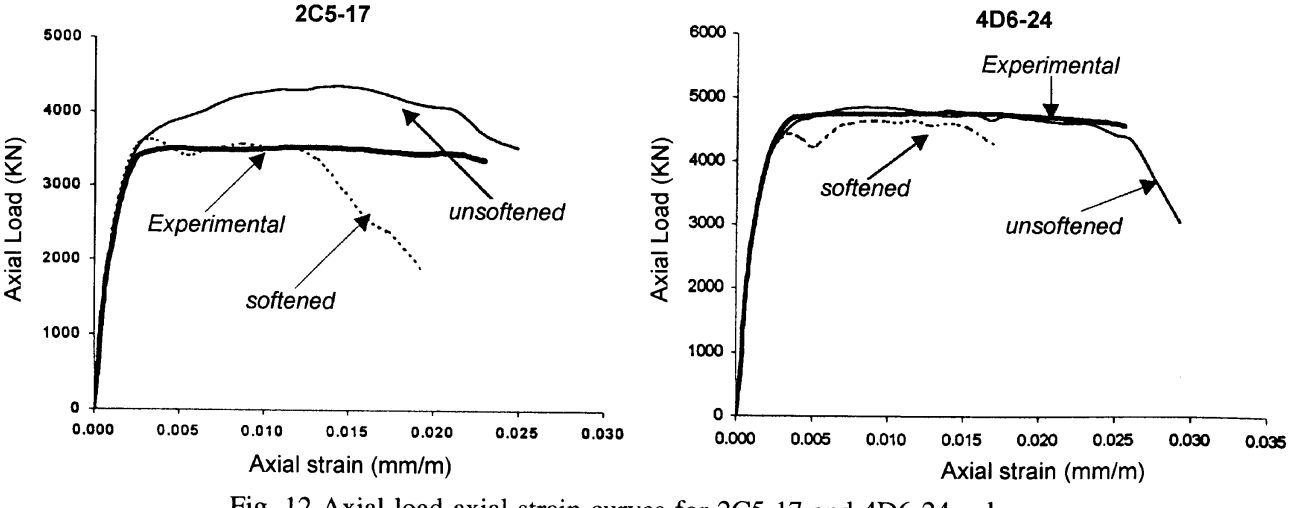

Fig. 12 Axial load-axial strain curves for 2C5-17 and 4D6-24 columns

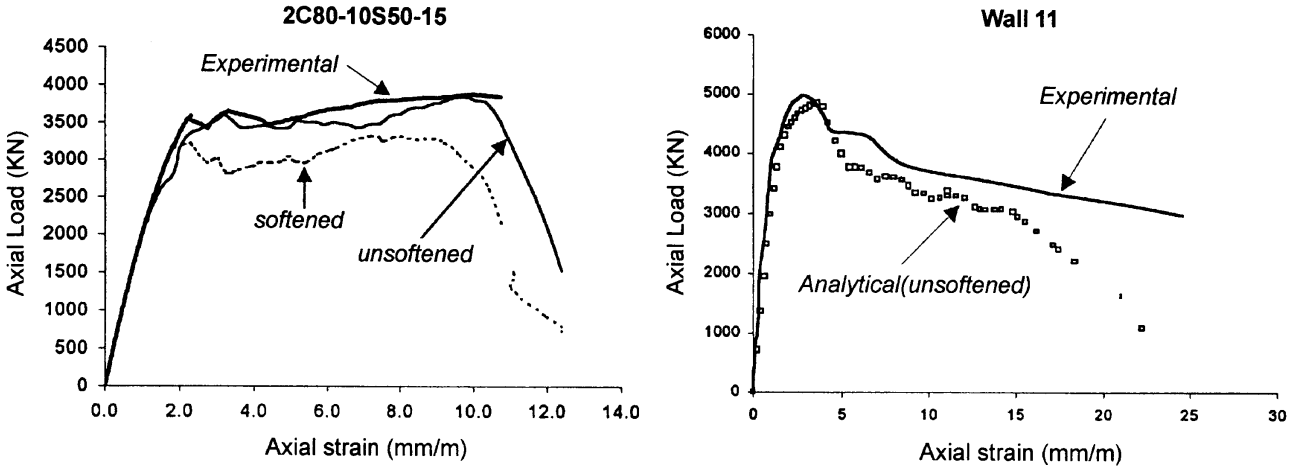

Fig. 13 Axial load-axial strain curves for 2C80-10S50-15 and Wall 11

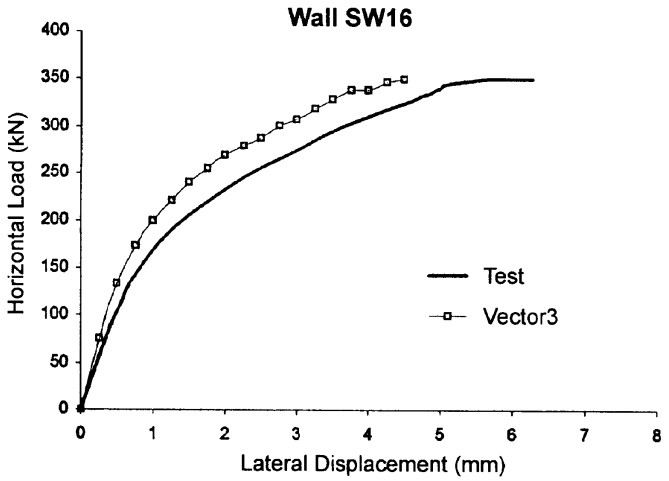

Fig. 14 Horizontal load-lateral displacement for wall SW16

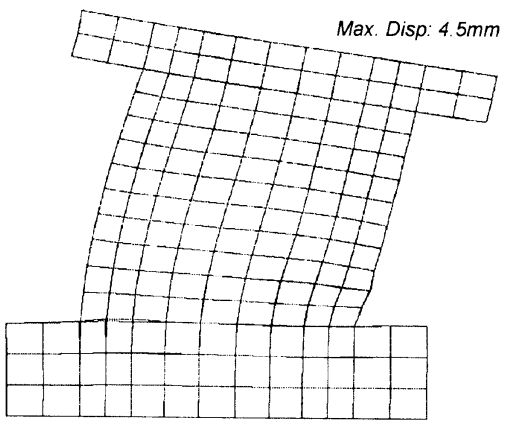

Fig. 15 Deformed shape at failure of Wall SW16

resistance was 355 kN). VecTor 3 underestimated the lateral displacement; perhaps because no attempt was made to model base rotation due to rebar slip. However; the analytical curve traced well the overall response of the wall. Flexural and flexural shear cracks developed at the top beam and the concealed column on the tension side. Shear cracks spread out into the wall web, and the bottom of the concealed column on the compression side was subjected to triaxial compressive stresses reaching a maximum principal compressive stress of 43 MPa (1.15 times 0.85 f_c').

5. Conclusions

The finite element program used for the corroboration of the experimental results is based on a nonlinear elastic approach which updates at every load or displacement step the material stiffness matrices of concrete elements and the equivalent forces due to prestrains (such as lateral expansion). Concrete material matrices are calculated as functions of secant stiffness values in the principal stress directions. Constitutive material behavior models for strength enhancement, lateral expansion, concrete softening, and post-peak ductility were examined using the program. The specimens studied represented different material and geometric properties. The results indicated that compression field modeling (smeared and rotating crack models) can be effectively used to represent the behavior of well- and poorly- confined concrete.

The material models used were found to accurately predict the strength and post-peak behavior of the specimens. It was noted that compression softening of concrete influenced the axial shortening response of the columns.

A squat shear wall with concealed columns, subjected to constant axial compression and monotonically increased lateral load, was modeled. It was found that triaxial compression stresses did occur at one of the concealed columns. The shear strength of the wall was predicted with good accuracy.

Nonlinear elasticity based on secant stiffness formulation is a viable alternative to fracture mechanics and plasticity models. The effect of stress-induced strains and offset strains can easily be considered in the solution of the equilibrium equations at the finite element level and the global stiffness matrix. Stresses in cracked concrete are considered orthotropic and computed from material behavior relationships which could be based on plasticity (or fracture mechanics) or empirical models, thus giving flexibility in the analysis.

Some advantages of this formulation are:

- Good transition between confined and unconfined concrete, and between core and cover concrete.
- Ability to effectively reproduce cover spalling, and to effectively model post-peak behavior of axially loaded columns with different geometry and steel arrangements.
- Good accuracy and stable numerical solutions.
- Provides potential for testing of empirical design formulations, and undertaking parametric studies.

6. Limitations, recommendations and future work

The analytical responses have an upper bound if softening of concrete is not included in the program options. If softening is included, a lower bound could occur as both ductility and strength decrease. Also, buckling of reinforcement in compression has not yet been implemented.

The following recommendations are made:

- The confinement model should be tested in specimens subjected to moment and axial load (i.e., eccentric loads).
- Improvement of the variable Poisson's ratio model to better model conditions beyond the 0.5 limit.
- Enhancement of the post-peak model for confined concrete in terms of triaxial stresses, to model ductility and failure conditions.
- Improvements to the tension behavior model for concrete to better model highly confined specimens with practically no cracking of the core.
- Improvements to the definition of lateral pressure in the confinement models to consider uneven triaxial compressive stress states, such as at the border of a concrete core near peripheral stirrups in a column.

Acknowledgements

The first author is grateful for the assistance provided by professors F.J. Vecchio and S.A. Sheikh of the University of Toronto. The financial support of the Natural Sciences and Engineering Research Council of Canada is also appreciated.

References

Chen W.F. (1982), *Plasticity in Reinforced Concrete,* McGraw-Hill, New York, N.Y.

Collins, M.P., and Mitchell, D. (1997), *Prestressed Concrete Structures,* Response Publications, Toronto, Canada.

Cusson, D., and Paultre, P. (1995), "Stress-strain model for confined high-strength concrete", *J. Struct. Eng.,* ASCE, **121**(3), 468-477.

Karabinis, A.I., and Kiousis, P.D. (1994), "Effects of confinement on concrete columns: Plasticity approach" *J. Struct. Eng.*, ASCE, **120**(9), 2747-2767.

Liu, J., Foster, S., and Attard, M. (1998), "Behaviour of tied high strength concrete columns loaded in concentric compression", Report No. R-372, The University of South Wales, Sydney, Australia.

Mander, B., Priestley, M.J.N., and Park, R. (1988), "Observed stress-strain behavior of confined concrete", *J. Struct. Eng.*, ASCE, **114**(8), 1827-1849.

Montoya, E. (2000), "Modeling of confined concrete", Master of Applied Science thesis, University of Toronto, Toronto, Canada.

Popovics, S.A. (1973), "Numerical approach to the complete stress-strain curve of concrete", *Cement and Concrete Research*, **3**(5), 553-599.

Pramono, E., and Willam, K. (1989), "Fracture energy-based plasticity formulation of plain concrete", *J. Eng. Mech.*, ASCE, **115**(6), 1183-1204.

Rasvi, S., and Saatcioglu, M. (1999), "Confinement model for high-strength concrete", *J. Struct. Eng.*, ASCE, **125**(3), 281-289.

Scott, B.D., Park, R., and Priestley, M.J.N. (1982), "Stress-strain behaviour of concrete confined by overlapping hoops at low and high strain rates", *J. American Concrete Institute,* **79**(1), 13-27.

Selby, R.G. (1990), *Nonlinear finite element analysis of reinforced concrete solids*, Master of Applied Science thesis, University of Toronto, Toronto, Canada.

Selby, R.G., and Vecchio, F.J. (1993), "Three-dimensional constitutive relations for reinforced concrete", Department of Civil Engineering Publication No. 93-02, University of Toronto, Toronto, Canada.

Selby, R.G., and Vecchio, F.J. (1997), "A constitutive model for analysis of reinforced concrete", *Canadian J. Civ. Eng.*, **24**, 460-470.

Sheikh, S.A., and Uzumeri, S.M. (1980), "Strength and ductility of tied concrete columns", *J. Struct. Div.*,

ASCE, **106**(ST5), 1079-1102.
Vecchio, F.J., and Collins, M.P. (1986), "The modified compression field theory for reinforced concrete elements subjected to shear", *J. American Concrete Institute*, **83**(2), 219-231.
Vecchio, F.J. (1992), "Finite element modeling of concrete expansion and confinement", *J. Struct. Eng.*, ASCE, **118**(9) 2390-2406.
Xie, J., MacGregor, J.G., and Elwi, A.E. (1996), "Numerical investigation of eccentrically loaded high-strength concrete tied columns", *ACI Struct. J.*, **93**(4), 449-461.